Monomeric and oligomeric forms of Bcl-xL in direct and indirect inhibition of apoptosis

Christina Elsner*[a], Daniel Roderer[b], Enrica Bordignon*[a]

[a] *Department of Physical Chemistry, Sciences II, University of Geneva, 30 Quai Ernest Ansermet, 1211 Geneva, Switzerland, E-mail: christina.elsner@unige.ch, enrica.bordignon@unige.ch,*

[b] *Leibniz-Forschungsinstitut für Molekulare Pharmakologie, Robert-Rössle-Str. 10, 13125 Berlin, Germany.*

The Bcl-2 protein Bcl-xL is a well-known inhibitor of apoptosis which can either directly inhibit the pore-forming Bcl-2 proteins, as Bax or Bak, or indirectly inhibit pore formation by sequestering the proapoptotic BH3-only proteins, as cBid or Bim. The structural basis of the inhibition of pore formation in the outer mitochondrial membrane by Bcl-xL is still largely unknown. Up to now, challenges in obtaining full-length Bcl-xL have hampered the full understanding of the inhibitory interactome at the membrane. Here we present an optimized protocol for the purification of full-length Bcl-xL, which allows separation of monomeric Bcl-xL from large oligomers which could not be otherwise eliminated in the purification procedure. The obtained monomeric Bcl-xL successfully inhibited pore formation via both modes of action, based on assays performed on large unilamellar vesicles in the presence of a minimal Bcl-2 interactome constituted by Bcl-xL, cBid and Bax. In contrast, the oligomeric fraction retained only the ability to indirectly inhibit pore formation by sequestering cBid. The presented protocol will pave the way towards biophysical studies aimed to unveil the structural details of apoptosis inhibition.

Introduction

The regulation of apoptosis is a major part of the body's development and prevention of diseases like cancer and Alzheimer's [1]. During the mitochondrial pathway of apoptosis this regulation is established by a fine balance between different members of the Bcl-2 protein family. At the center of this protein family are effector or pore-forming proteins (Bax or Bak) that cause mitochondrial outer membrane permeabilization (MOMP) by pore formation. Whether or not this process can occur, is fine-tuned by either pro-apoptotic BH3-only proteins (such as cBid, Bim, etc.) that activate the pore formation or by anti-apoptotic proteins (such as Bcl-xL, Bcl-2, etc.) that prevent the pore formation. In the complex interplay between these three sub-groups of the Bcl-2 protein family there is another important player: the mitochondrial outer membrane (MOM). Both protein-protein and protein-membrane interactions will ultimately decide the fate of the cell. [2, 3]

For the inhibition of apoptosis by Bcl-xL, three different modes of action have been described. Mode 1 suggests a shift in equilibrium between membrane-bound and soluble Bax caused by Bcl-xL. Mode 2 suggests direct inhibition of pore-formers by heterodimerization with Bcl-xL. Mode 3 describes an indirect inhibition of apoptosis by binding activators like cBid (cleaved Bid consisting of p7 and tBid which contains the BH3 domain) and thereby preventing activation of the pore formers.[3–5] This mode is especially interesting, since it has been shown that Bcl-xL has a higher affinity to BH3-only proteins than to pore formers [2].

The Bcl-2 interactome is regulated by diverse interactions between the Bcl-2 homology (BH) domains. As their name implies, BH3-only proteins possess only the BH3 domain and are mostly intrinsically disordered (with the notable exception of (c)Bid)[6]. Both pore formers and inhibitors have four conserved BH domains (1-4) and an additional C-terminal transmembrane helix which is often cleaved off (ΔC variants) in recombinant proteins used for in vitro studies (in particular for Bak and Bcl-xL). Their fold shows a hydrophobic groove assembled by the BH domains 1-3, which was shown to efficiently bind BH3 motifs of other Bcl-2 proteins. [7] This BH3-to-groove interaction is responsible for most homo- and hetero-interactions within this protein family. However, other interaction sites have been discovered, e.g. full-length Bax and Bcl-xL showed an additional interaction interface between their respective α1-helices [8], and water soluble domain-swapped Bax or Bcl-xL-ΔC homodimers interacted through three-dimensional domain swapping, leaving the BH3-binding groove accessible for additional interactions [9, 10].

In vitro analysis was performed using full-length Bcl-xL in few cases [11, 12] but most structural work was conducted on various different Bcl-xL deletion-variants. In particular, the structure of Bcl-xL in water was solved by NMR on a ΔC variant (PDB entry 1LXL, (see fig

1 A)), the BH3-to-groove binding was characterized on deletion-variants of the long loop region of Bcl-xL (e.g. Δ45-84) and of the C-terminal transmembrane domain (e.g. Δ212-233), in complex with peptides derived from BH3-domains (see e.g. PDB entries: 4QVE, 1BXL, 1G5J, 3FDL, 4CIN). It still remains to be elucidated whether the results obtained on truncated Bcl-xL variants in solution can be directly correlated to the properties of full-length proteins in the presence of the mitochondrial membranes. Up to date, there exists only one structural study of full-length monomeric Bcl-xL in solution and anchored to nanodiscs (see fig 1 A) , which was obtained using a combination of NMR spectroscopy and MD simulations [13]. However, with both truncated and full-length Bcl-xL, the formation of dimers and higher order oligomers has been described (see fig 1 A) and their role in apoptosis, membrane alteration and calcium homeostasis was discussed. [9, 11, 14–16]
In this work we present an optimized Bcl-xL purification protocol based on a previously published one [12], which allows efficient separation of the monomeric full-length human Bcl-xL protein from its oligomeric form (in the following named Bcl-xL^{O}). The detailed characterization of monomers and oligomers of Bcl-xL demonstrated that they both have the BH3-binding groove accessible for binding to the BH3 domain of cBid, but while the full-length monomeric Bcl-xL performed both direct and indirect inhibition of membrane permeabilization, Bcl-xL^{O} only retained the ability to inhibit cBid.

Results

Characterization of Bcl-xL: monomers and oligomers

We purified full-length (res. 1-233) human Bcl-xL adding a third purification step to a previously published protocol[12]. We used a Bcl-xL construct containing a cleavable C-terminal intein tag with a chitin binding domain, which was already successfully used to purify full-length Bcl-xL [11, 13]. The first step of purification was performed using chitin beads, which was followed by an anion exchange column. A final size exclusion chromatography was added as third purification step (the detailed 3-step purification protocol is described in the materials & methods), which yielded two well separated forms of Bcl-xL: a monomeric form (confirmed by an elution peak corresponding to 26 kDa molecular weight, see fig 1 B) and an oligomeric form (eluting in the void volume in the Superdex 75 in see fig 1 B), that was further characterized to be >200 kDa with a Superdex 200 (see SI) and mass photometry (see fig 1 C). Notably, in buffers at pH 7.5 the isolated monomeric fraction collected at a concentration of around 1 μM after the SEC was stable and could be concentrated in centrifugal units (either Amicon or Vivaspin) to 10-20 μM without protein losses.

To further characterize the properties of Bcl-xL^{O}, we performed a mass photometry anal-

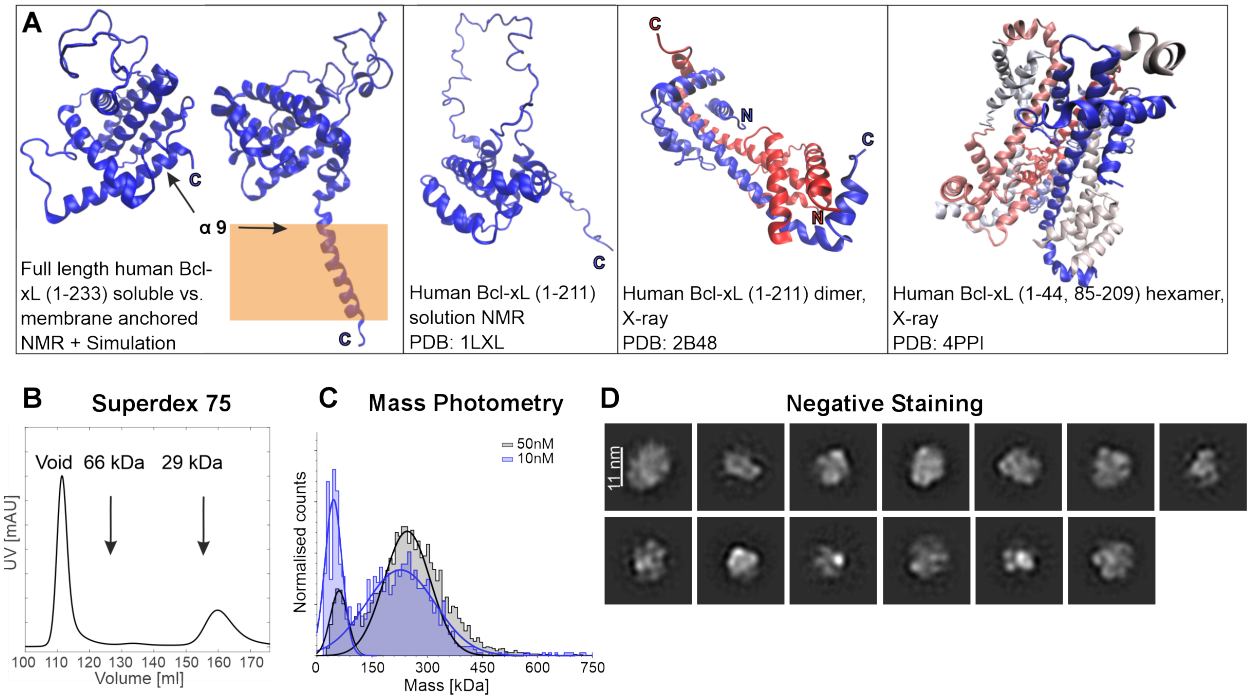

Figure 1: Monomeric, dimeric and oligomeric forms of Bcl-xL. A: Examples of Bcl-xL structures. From left to right: full-length Bcl-xL in aqueous and nanodisc environment obtained by NMR and MD simulations[13]; NMR structure of monomeric Bcl-xLΔC in solution; crystal structure of a water-soluble dimer of Bcl-xLΔC formed by 3D-domain swapping; crystal structure of a water-soluble hexamer of Bcl-xLΔC-Δloop formed by domain-swapped dimers. **B:** Size exclusion profile from our Bcl-xL purification protocol performed on a Superdex 75 26/600 column at 4°C. Arrows indicate reference protein elution volumes. The peak eluting in the void volume corresponds to Bcl-xL^{O} (size >70 kDa), the peak eluting at 160 ml (just after a reference protein of 29 kDa) corresponds to monomeric Bcl-xL (26 kDa). An additional SEC profile (Superdex 200) is shown in the SI. **C:** Mass photometry of Bcl-xL^{O} diluted to 10 nM (blue) and 50 nM (grey) (protomer concentrations). For the 10 nM sample, we found a low-molecular-mass peak (at the mass sensitivity limit of the method) centered around 45 kDa (σ=23 kDa, 349 counts, 34%) and a high-molecular-mass peak at around 228 kDa (σ=95 kDa, 783 counts, 77%). For the 50 nM sample, the low-molecular-mass peak is centered around 60 kDa (σ=24 kDa, 1000 counts, 14%) and the high-molecular-mass peak centered around 240 kDa (σ=82 kDa, 4120 counts, 81%). **D:** 2D class averages of 1712 particles of negative stain data obtained on Bcl-xL^{O}. The size and shape of the observed particles are compatible with tetramers. Additional data in the SI.

ysis on isolated Bcl-xL^{O} at 10 and 50 nM protomer concentration (after dilution of the fraction collected at 5 μM protomer concentration after SEC). The main peak centered at about 230-240 kDa (see fig 1C) was characterized by a broad distribution of masses, indicating the existence of a mixture of various different high order oligomers in the sample. Bcl-xL^{O} could not be concentrated in centrifugal units due to protein aggregation and losses. Interestingly, we found that isolated Bcl-xL^{O} when diluted to nanomolar concentrations can partially dissociate into smaller complexes with a molecular mass of about 50 kDa (see fig. 1 C). Since monomeric Bcl-xL (26 kDa) is below the detection limit of mass photometry, we cannot unambiguously assign the smaller mass fraction to dimers or monomers. We then subjected isolated Bcl-xL^{O} to negative stain electron microscopy (NS-EM) and observed predominantly 10 nm wide and compact shaped particles, but also a fraction of smaller particles (SI Fig. 1D). 2D classification revealed that a majority of particles (1712 out of 3404 extracted particles) was sorted in 13 classes that represent large particles with 10 - 12 nm diameter, most of them compatible with Bcl-xL tetramers in size and shape (Fig. 1D). In addition, 1380 particles were sorted into 18 classes that represent small particles, compatible with Bcl-xL monomers (SI Fig. 1E). This indicates a considerable level of instability of the higher order complexes formed by Bcl-xL during the purification procedure.

Direct and indirect inhibition of apoptosis: Bcl-xL monomers vs oligomers

The ability of the purified Bcl-xL fractions to perform direct and indirect inhibition of Bax-induced pore formation was probed on large unilamellar vesicles (LUVs) using an in-vitro fluorescence-based pore formation assay, that monitors the leakage of a highly concentrated, self-quenching fluorophore from the LUVs, following pore formation by Bax (see materials & methods). We used a minimal Bcl-2 interactome consisting of cBid, Bax, and either monomeric Bcl-xL or Bcl-xL^{O}. To monitor both the direct and indirect inhibition modes of Bcl-xL, the Bax-to-lipid ratio was optimized to reach 40% membrane permeabilization by Bax alone (autoactivity, dark grey dashed lines in fig. 2A) and 80% permeabilization by cBid-induced Bax activity (stoichiometric ratio 1:1) (light grey dashedd lines, in fig. 2A). If either monomeric or oligomeric Bcl-xL is combined with Bax and cBid (1:1:1 protein ratio) the 80% permeabilization is decreased to around 40%, very close to Bax autoactivity (cyan and light purple in fig. 2A), indicating that both forms of Bcl-xL effectively inhibit cBid in a 1:1 stoichiometric ratio (for the oligomers, we consider the protomer stoichiometry). When monomeric Bcl-xL is added in a 1:1 ratio to Bax alone, the fluorophore leakage is decreased to <10% (blue in fig. 2A), indicating almost full inhibition of Bax autoactivity (direct mode of inhibition). In contrast, when Bcl-xL^{O} is added, no inhibition of Bax autoactivity could be

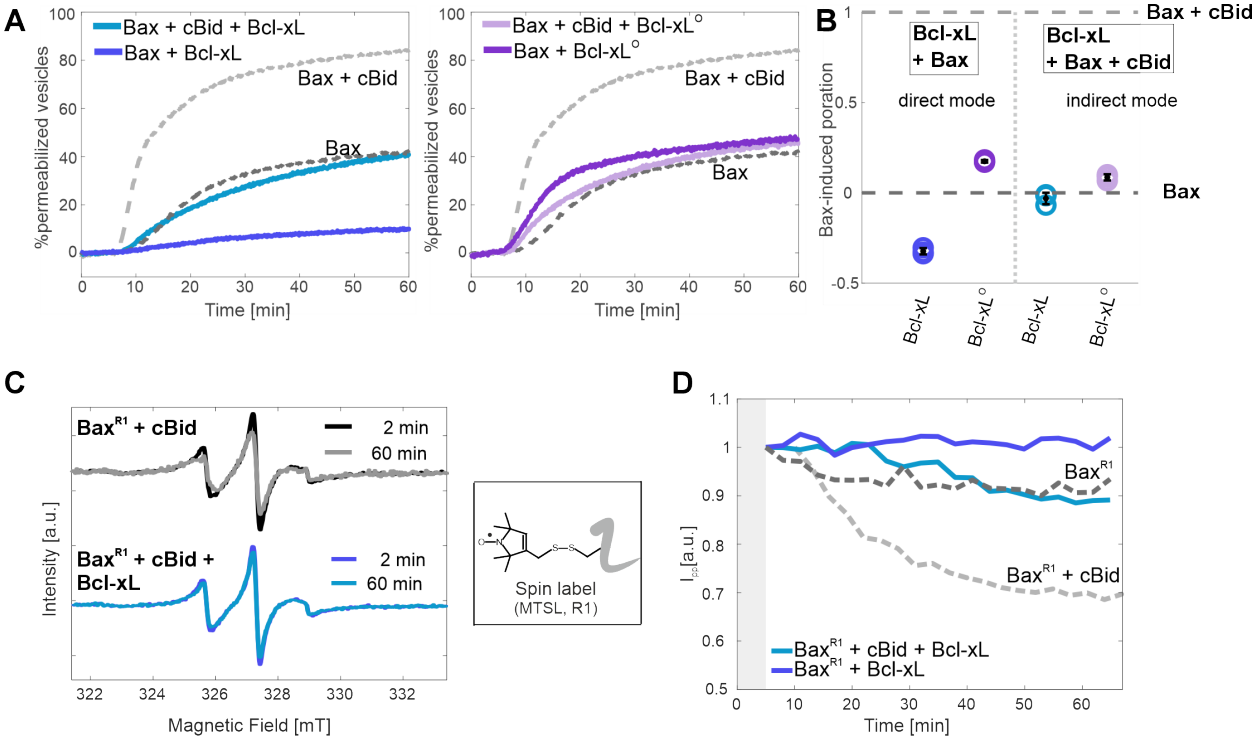

Figure 2: Inhibition modes of monomeric and oligomeric Bcl-xL. A: Examples of pore formation assays based on the release of the fluorescent probe calcein from LUVs through Bax-induced pores. The time traces show the amount of permeabilized vesicles at 37°C over time, normalized to the highest release of fluorescent probes from LUVs induced by lysis with detergents (100%) (see materials & methods and SI) . All proteins were added at a concentration of 25 nM. The dotted lines on the two graphs show reference measurements (Bax alone, dark grey, 40% autoactivity; Bax + cBid, light grey, 80% activity). Left: monomeric Bcl-xL completely inhibits Bax autoactivity from 40% to 10% (from dashed dark grey to blue) proving the direct mode of inhibition and decreases the cBid-induced activity from 80% to 40% (from dashed light grey to cyan), proving the indirect mode of inhibition. Right: the inhibitory effects of Bcl-xL^{O} on cBid-induced activity (from dashed light grey to light purple) prove the indirect mode of inhibition of Bcl-xL^{O}. Bax autoactivity (dashed dark grey) cannot be directly inhibited by Bcl-xL^{O} (purple). **B:** Statistical comparison (3 technical replicates) of the inhibitory effects of Bcl-xL monomer and oligomer after 30 min of incubation. The value 1 represents the normalized maximal Bax activity (permeabilization achieved by activated pore formation Bax + cBid) and 0 represents the permeabilization caused by Bax autoactivity. **C:** Direct and indirect inhibition of monomeric Bcl-xL proven by EPR. Examples of continuous wave X-band EPR spectra of Bax spin-labeled at the two natural cysteines with the methanethiosulfonate spin label MTSL (named Bax^{R1}). When Bax^{R1} at micromolar concentrations is incubated at 37°C with LUVs and cBid (1:1 protein stoichiometric ratio) the spectral intensity decreases (2 min incubation, black and 60 min incubation, light grey) due to Bax oligomerization and membrane insertion. In the presence of Bcl-xL (1:1:1 ratio) only minimal spectral changes are detected (2 min incubation, blue and 60 min incubation, cyan). The inset shows the MTSL spin label attached to a cysteine yielding the residue R1. **D:** EPR kinetics of the membrane insertion of Bax^{R1} obtained by plotting the peak-to-peak intensity of the spectra over time. Both the cBid-induced Bax activity (light grey, dashed) and the Bax autoactivity (dark grey, dashed) are inhibited by monomeric Bcl-xL (cyan and blue, respectively), confirming the fluorescence data shown in panels A and B. Bcl-xL^{O} could not be tested due to concentration restraints.

observed (dark purple in Fig. 2A), indicating that Bcl-xL^{O} lost the ability to directly inhibit Bax. Figure 2B summarizes the results on three technical repeats. The y-axis represents a normalized Bax activity, with the value 1 indicating the maximal membrane poration achieved by fully activated Bax (with cBid), the value 0 indication the poration induced by Bax autoactivity. For an efficient direct inhibition mode by Bcl-xL, the value of Bax activity should go below zero, which is achieved only with monomeric Bcl-xL. For an efficient indirect inhibition mode, the Bax activity should go to zero (cBid is inhibited, therefore only the autoactivity of Bax is retained), which is found for both monomeric and oligomeric Bcl-xL fractions. The data demonstrate that the purified monomeric full-length Bcl-xL retains the ability to inhibit cBid as well as Bax at molar stoichiometric ratios, while Bcl-xL^{O} retains only the indirect mode of action.

To corroborate the conclusions drawn by fluorescence assays that Bcl-xL monomers can efficiently act in both inhibitory modes, we performed an additional activity assay using spin-labeled wild type Bax (labeled at its natural cysteines 62 and 126 with the spin label MTSL and called for simplicity Bax^{R1}) at micromolar concentrations and continuous wave (cw) electron paramagnetic resonance (EPR) spectroscopy. By monitoring the changes of the EPR spectrum of Bax^{R1} over time in presence of LUVs and Bcl-2 partners (fig. 2C), we can follow Bax membrane insertion and oligomerization, as previously shown [17, 18]. The EPR spectrum becomes broader (therefore the peak-to-peak spectral intensity decreases) when the label's rotational dynamics are slowed down e.g. when Bax enters the membrane and/or oligomerizes (fig. 2C). Analyzing the peak-to-peak intensity (Ipp) of the spectra allows following the kinetics of membrane insertion and protein oligomerization which induces pore formation (fig. 2D). When Bax^{R1} is mixed with LUVs the spectral peak-to-peak intensity drops to 90% of its initial value due to Bax' autoactivity (dark grey dashed line in fig. 2D). If Bcl-xL monomers are added in a 1:1 stoichiometric ratio to the mixture, no spectral changes are observed (fig. 2D, blue line), further confirming the efficient direct inhibition mode of monomeric Bcl-xL. When Bax^{R1} and cBid (1:1) are mixed with LUVs, the peak-to-peak intensity drops to around 70% of the starting intensity within one hour (dark grey dotted line in fig. 2D). If Bcl-xL monomers are added to the mixture in a 1:1:1 ratio, the spectral changes reach only the Bax autoactivity level (90%) in one hour (cyan line in fig. 2D), confirming that monomeric Bcl-xL efficiently performs also the indirect mode of inhibition, corroborating the fluorescence data. The fluorescence and EPR activity assays demonstrate that the purified monomeric full-length Bcl-xL retains the ability to inhibit cBid as well as Bax both at nanomolar (pore formation assays) and at micromolar (EPR assays) concentrations in a 1:1 ratio to Bax or cBid. Bcl-xL^{O} however cannot inhibit Bax directly, but retains the ability to inhibit cBid.

Water-membrane partitioning of Bcl-xL monomers and interactions with Bcl-2 partners

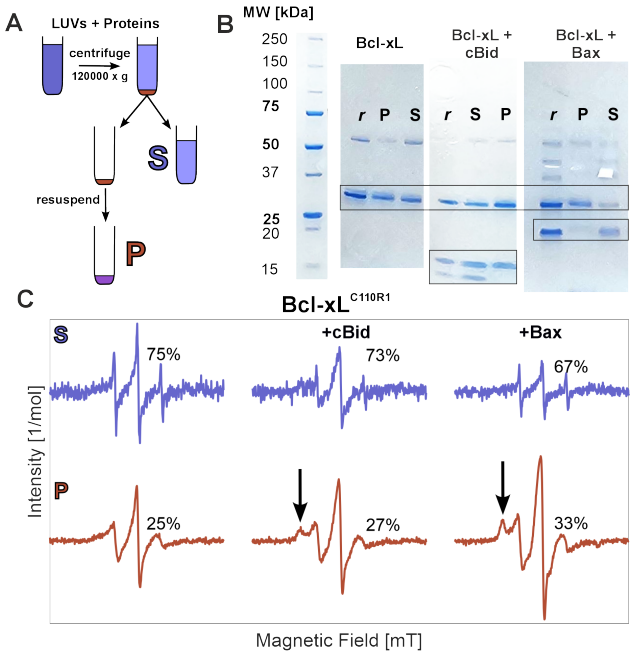

Figure 3: Membrane affinity of monomeric Bcl-xL. A: Schematic description of the sample preparation. The protein-LUV mixture is incubated for one hour at 37°C before being separated by centrifugation. The supernatant is separated from the pellet, which is resuspended in buffer. **B:** SDS PAGE analysis of different combinations of full-length Bcl-2 proteins with and without LUVs; r: reference protein sample in solution without LUVs. S, P: supernatant and pellet samples prepared as described in A. Boxes highlight bands corresponding to monomeric Bcl-xL (26 kDa, all panels), cBid (tBid and p7 bands at 15 and 7 kDa, respectively, middle panel) and Bax (21 kDa, right panel). Bands at higher masses are caused by residual homo- and hetero-dimers formed in the absence of reducing agents. **C:** EPR spectra of the supernatant and pellet fractions obtained from mixtures of LUVs with Bcl-xL^{C110R1} alone (left) or in combination with cBid (middle) or Bax (right) in a 1:1 stoichiometric ratio. The percentages indicate the relative amount of moles (10% estimated error) of spin-labeled Bcl-xL in each fraction (obtained from the calculated area of the EPR spectra and the volume of each fraction). The arrows point to spectral changes caused by the interaction of Bcl-xL with Bcl-2 partners in the membrane.

Having determined that monomeric Bcl-xL is fully functional in both modes of inhibition, we characterized its partitioning between aqueous solution and membrane environment using SDS-PAGE and EPR spectroscopy. In addition, we studied the effect exerted on the water-membrane equilibrium of Bcl-xL by other Bcl-2 partners, namely cBid and Bax. To quantify the amount of Bcl-xL in both environments, we used a simple centrifugation method. We incubated Bcl-xL and LUVs in the presence or absence of cBid or Bax for one hour at 37°C, followed by separation of the mixture via centrifugation. The pellet (P) and supernatant (S) fractions were separately analyzed (see Fig. 3A). As reference (r), we used the same

protein mixture in the absence of LUVs. The SDS PAGE analysis shown in Fig. 3B shows the division of monomeric Bcl-xL in a water and a membrane-bound fraction. The presence of cBid does not further affect the ratio of these fractions. Notably, in the supernatant both bands of the cleaved cBid (tBid, 15 kDa and p7, 7 kDa) can be detected, however, the pellet fraction shows only tBid. If full-length Bax is present, we observed an increased accumulation of Bcl-xL in the pellet while Bax can be mainly found in the supernatant.
To corroborate the partitioning found in SDS PAGE and additionally investigate the dynamics of Bcl-xL in the supernatant and in the pellet fractions, we used a spin-labeled Bcl-xL variant, carrying the MTSL label at position 110 (called for simplicity Bcl-xL^{C110R1}). The spin-labeled side chain R1 is located in the hydrophobic groove of Bcl-xL, which was previously shown to bind BH3-peptides[9, 15]. The EPR spectra of Bcl-xL^{C110R1} were recorded in the supernatant and pellet fractions prepared as in 3A, and the double integral of the EPR spectra was calculated, which is proportional to the concentration of Bcl-xL^{C110R1}. Thanks to the label quantification by EPR, we could calculate the percentage of moles of labeled Bcl-xL present in each fraction (Fig. 3C). We found that 25% of the total amount of Bcl-xL monomers binds to the membrane which remains unchanged in the presence of cBid. However, in the presence of Bax the amount of membrane-bound Bcl-xL increased to 33% in line with the resulty from SDS PAGE (Fig. 3B). Notably, the spectral shape of Bcl-xL in the membrane changed when cBid or Bax were present during incubation. The arrows in Fig. 3C highlight the spectral component emerging in the presence of the Bcl-2 partners, which indicates that the label in Bcl-xL^{C110R1} has slower rotational dynamics due to changes induced by tBid or Bax. This is especially interesting because this label is positioned within the BH3-binding groove of Bcl-xL and the spectral change indicates additional sterical hindrance slowing down the rotational dynamics of the spin-labeled residue 110, possibly caused by a direct interaction with the other Bcl-2 interaction partner (formation of an heterocomplex) and/or by structural changes within Bcl-xL triggered by the presence of the interaction partner.

BH3-to-groove Interaction

The full-length monomeric Bcl-xL in water has the trans-membrane helix 9 covering the hydrophobic groove, but in the membrane-bound structural model previously published [13] the groove is available for interaction with BH3 domains. To test if the membrane-bound form of the monomeric Bcl-xL has the hydrophic groove at disposal for interactions with the BH3 domain of tBid, we used the spin-labeled Bcl-xL variant carrying the MTSL label at C110 (in the hydrophobic groove) and we added another singly-labeled cBid variant carrying the MTSL label at position 82 (in the BH3 domain) (see Fig. 4A). The two spin-labeled

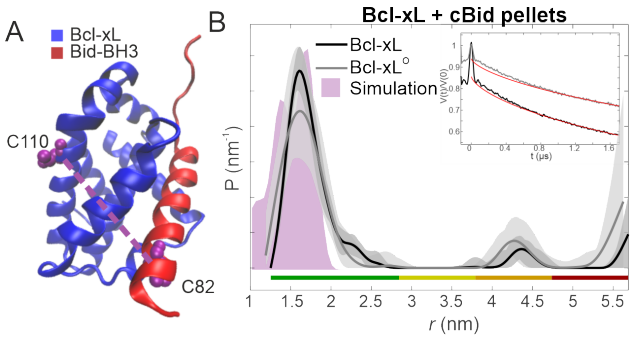

Figure 4: BH3-groove interaction in membranes. A: Protein crystal structure from PDB 4QVE showing the water-soluble complex between Bcl-xLΔCΔloop and a BH3-peptide from Bid. The positions 110 in Bcl-xL and 82 in the BH3-peptide are highlighted. **B:** DEER distance measurements between cBid^{C82R1} (label in the BH3 domain) and Bcl-xL^{C110R1} (label in the BH3-binding groove) in LUVs (black: monomeric Bcl-xL and grey: oligomeric Bcl-xL; the shaded grey areas represent the uncertainties) compared with the simulated distance distributions obtained with MMM[19] (purple area) based on the PDB 4QVE. The inset shows the DEER primary data.

proteins were incubated with LUVs and the pellet was prepared as in Fig. 3A. Based on the available crystal structure of the water-soluble complex between Bcl-xLΔCΔloop and a BH3 peptide from Bid (PDB: 4QVE, see Fig. 4A), the two labels should be at a distance of about 1.5 nm, as predicted by the rotamer analysis software MMM [19]. To obtain the distance between the spin label in Bcl-xL (groove) and the spin label in tBid (BH3 domain) in the membrane fraction, we used a pulsed dipolar spectroscopy sequence called Double Electron Electron Resonance (DEER, aka PELDOR[20]). The experimental distance obtained on the pellet fraction is centered at 1.6 nm (see Fig. 4B). The experimental distance is in very good agreement with the distance simulated on the crystal structure (black versus shaded purple area in Fig. 4B). This finding confirms the inhibitory BH3-groove interaction at the membrane between tBid and Bcl-xL. Interestingly, spin-labeled Bcl-xL^{O} showed the same 1.6 nm distance to the BH3-domain of tBid in the pellet fraction (black versus grey distance distribution in Fig. 4B), proving that at the membrane both Bcl-xL monomer and oligomer can bind the BH3-domain of tBid in their BH3-binding groove. This result is in agreement with the efficient indirect mode of inhibition exerted by both Bcl-xL forms (Fig. 2). The DEER data (Fig. 4) unveil that in the presence of a membrane environment, the hydrophobic groove of Bcl-xL is accessible to the BH3 domain of tBid, proving the structural origin of the indirect inhibition observed via fluorescence and EPR assays in presence of Bax, cBid, and LUVs (fig. 2). Notably, the accessibility of the groove is not sufficient for the direct inhibition of Bax, because Bcl-xL^{O} retains the ability to bind the BH3 domain of tBid, but it is not able to directly inhibit Bax (see Fig. 2) suggesting a more complex mode of interaction between Bcl-xL and Bax, which can be efficiently created only by the monomeric form of Bcl-xL.

Discussion

The presented optimized purification protocol of recombinant full-length Bcl-xL yielded a pure, fully active water-soluble monomeric Bcl-xL well separated from a fraction of higher order oligomers. The monomeric Bcl-xL was proven to execute both direct and indirect modes of inhibition, as shown by in vitro assays using a minimal interactome consisting of Bcl-xL, cBid, and Bax. Once isolated, the monomeric fraction of Bcl-xL is stable, and can be concentrated up to 10-20 μM, without spontaneous re-formation of oligomers in pH 7.5 aqueous buffers. In contrast, the high order oligomers isolated from the purification protocol presented here were shown to easily aggregate on centrifugal devices and to partially dissociate into smaller units at nanomolar concentrations or when stained on grids for electron microscopy. It is therefore conceivable that they cannot be stable at the physiological nanomolar concentrations in cells. However, the propensity of truncated variants of Bcl-xL to form dimers and higher-order oligomers and the difficulty in avoiding large oligomers when purifying full-length Bcl-xL prompted speculations about a possible role of oligomers in the inhibition of apoptosis. Indeed, it was shown for the 3D domain-swapped (3DDS) dimer formed by truncated Bcl-xL variants, that the BH3-binding groove remains accessible to BH3 peptides[15], which is sufficient to retain the ability to indirectly inhibit pore formation via sequestration of BH3-only proteins by Bcl-xL dimers and oligomers. We show here that the groove of full-length Bcl-xL oligomers can still bind the BH3 domain of tBid in the membrane, analogously to the monomeric form of membrane-embedded Bcl-xL. This explains why both monomers and oligomers can sequester tBid and indirectly inhibit apoptosis. However, to perform the direct inhibition of Bax or Bak, the availability of the hydrophobic groove might not be sufficient and more stringent conditions need to be fulfilled. The affinity of the BH3-binding groove for a Bak-BH3-peptide was found to be about half for dimeric and oligomeric Bcl-xL compared to monomeric truncated Bcl-xL[9]. The lower affinity of oligomeric Bcl-xL for a pore-former (Bak) BH3-peptide together with the existence of a secondary Bax-Bcl-xL interaction site via their two α1-helices[8] might give an indication as to why the full-length Bcl-xL oligomer is not able to directly inhibit Bax autoactivity despite being able to inhibit activation of Bax by sequestering tBid.

In cells, the affinity of Bcl-xL towards the different Bcl-2 partners is key to maintain cellular homeostasis. In literature, Bcl-xL is mostly used in excess to cBid to achieve full cBid inhibition (see for example [11, 12]). In this work we obtained fully active Bcl-xL monomers, which efficiently inhibit Bax or cBid at exactly 1:1 stoichiometric ratios, indicating that in cells a 1:1 ratio might be sufficient for inhibition. Based on all data presented, we favor the use of monomeric full-length Bcl-xL for future biophysical studies of the inhibitory complexes at the MOM. We demonstrate here that, using EPR, it is possible to identify the BH3-to-groove

interaction formed in the Bcl-xL-tBid complex at the membrane, corroborating previous results obtained with truncated Bcl-xL variants and BH3-peptides in aqueous solutions. In addition, we identified a dynamic change in the hydrophobic groove of membrane-embedded Bcl-xL not only in presence of tBid, but also in the presence of Bax, which gives first hints towards the Bcl-xL-Bax inhibition mechanism.

Conclusion

In this work we describe an optimized purification protocol to separate the monomeric, fully active human Bcl-xL from its oligomeric form. The monomeric Bcl-xL executes both direct and indirect inhibition of membrane permeabilization in a 1:1 stoichiometric ratio with the Bcl-2 partners, as shown with a minimal Bcl-2 interaction network in vitro. In contrast, isolated Bcl-xL^{O} retained only the ability to inhibit cBid. The indirect inhibition is due to the interaction of the BH3 domain of tBid with the hydrophobic groove of membrane-embedded Bcl-xL, which is exposed in both monomeric and oligomeric membrane-embedded forms of Bcl-xL. However, the absence of direct inhibition of Bax autoactivity by Bcl-xL^{O} strongly suggests that the mere accessibility of the BH3-binding groove is not sufficient to directly inhibit Bax. This work paves the way towards a detailed biophysical analysis of the inhibitory complexes formed by Bcl-xL and tBid or Bax at the membrane, that will ultimately unveil the structural basis of the regulatory mechanisms of Bcl-2 proteins in the mitochondrial pathway of apoptosis.

Methods

Expression of recombinant proteins

The plasmids of pTYB1-Bcl-xLC110 (S110C-C151S) and pET23d-BidC82 (C30S-S82C-C126S) were cloned by site-specific mutagenesis and controlled via DNA sequencing. His-tagged mouse Bid (pET23d[21]), human Bax (pTYB1[22]), and human Bcl-xL (pTYB1[12], kindly provided by Prof. Garcia-Saez) were expressed in E. coli and induced with IPTG 4h (Bid) or overnight (Bcl-xL, Bax), respectively, and the pellets were either used immediately or shock frozen in liquid nitrogen and stored at -80°C. After lysis of the bacteria in a microfluidizer and incubation with 1-200U DNase I per liter of bacterial culture, the membranes and intact bacteria were separated from the soluble fraction via centrifugation at 35000xg for 35 min.

Purification, cleavage, and spin labeling of Bid

Bid was purified from the soluble fraction of the bacterial lysate using Ni-NTA (Ni-NTA Superflow by Qiagen). It was washed first with Nickel buffer (20 mM Tris, pH 7.5, 20 mM NaH2PO4, 300 mM NaCl) without imidazole, then with 10 mM and 25 mM before being eluted with 250 mM imidazole. The protein was stored in storage buffer (20 mM Tris, pH 7.5, 150 mM NaCl).
Bid (100-150 µM) was mixed 1:1 with cleavage buffer (50 mM HEPES, pH 7.5, 100 mM NaCl, 10 mM DTT, 1 mM EDTA, 10% sucrose) and Caspase 8 (final concentration 1 µM). The mixture was incubated for 3 h at room temperature and purified using Ni-NTA, washed with Nickel buffer without imidazole, eluted with 250 mM imidazole and dialyzed back into storage buffer. The cleaved Bid is called cBid in the following.
For spin labeling with MTSL, cBid was diluted to 10-20 µM and incubated with 1 mM DTT for 1 h. After removal of DTT in a desalting column, Bid was immediately mixed with 10x excess MTSL and incubated at 8°C overnight. Excess label was removed in a desalting column. The spin labeling efficiency (spin per protein) of $cBid^{C82R1}$ was 44%, as calculated by comparing the second integral of the cw EPR spectra with a reference TEMPOL standard (see SI).

Purification and spin labeling of Bcl-xL and Bax

Bcl-xL and Bax were purified from the soluble fraction of the bacterial lysate using chitin resin (New England Biolabs) which was washed 20x with chitin buffer (20 mM Tris (Bcl-xL) or 8 mM Tris (Bax), pH 8.0, 500 mM NaCl) and 3x cleavage buffer (chitin buffer + 30 mM DTT freshly added). The column was filled with cleavage buffer, closed and incubated at 4°C overnight to cleave off the intein tag. The proteins were eluted with chitin buffer and dialyzed 1:10 against 20 mM Tris (pH 8.0) with one step (Bcl-xL) or 8 mM Tris (pH 8.0) in five steps (Bax), respectively.
For Bcl-xL, 1 mM DTT was added to the dialysate before loading on an anion exchange column (POROS™ GoPure™ 50 HQ Pre-packed Column) at 0.5 ml/min. The column was washed with Mono A50 buffer (20 mM Tris, pH 8.0, 50 mM NaCl, 1 mM DTT) and the protein was eluted running a gradient with Mono B buffer (20 mM Tris, pH 8.0, 1 M NaCl, 1 mM DTT). The pooled fractions of the main peak were injected into a size exclusion column (Superdex 200 10/300) equilibrated with storage buffer. If the protein had to be labeled afterwards, 10 µM TCEP was freshly added to the storage buffer. The resulting oligomer peak was pooled but not concentrated as centrifugal filters cause the oligomers to aggregate. The monomer peak was pooled and concentrated in centrifugal filters (Vivaspin® Turbo 4

Sartorius (cutoff 10 kDa)). During the optimization procedure, we found that skipping the anion exchange column and perform directly the SEC resulted in significantly higher amount of monomers with respect to oligomers; however the resulting monomers were less active (if the SEC was performed at pH 8.0) or even completely inactive (SEC at pH 7.5) monomers. To label the monomeric fraction of Bcl-xL, 5-10x excess MTSL was added per protein (protein concentration 10-20 µM) and incubated overnight at 8°C. The excess label was removed by washing 4-5x in centrifugal filters (Vivaspin® Turbo 4 Sartorius (cutoff 10 kDa)) with storage buffer. The spin labeling efficiency (spin per protein) of monomeric Bcl-xL^{C110R1} was 49%, as calculated by comparing the second integral of the cw EPR spectra with a reference TEMPOL standard (see SI).
To label the oligomeric fraction, it was dialyzed (Pur-A-Lyzer™ Mini Dialysis) against storage buffer to decrease the TCEP concentration. Then, 0.25x MTSL per protein (protomer concentration) was added and incubated first for 30 min at room temperature and afterwards for 1.5 h at 4°C. To remove the excess label, the solution was dialyzed against storage buffer overnight at 4°C. The spin labeling efficiency (spin per protein) of oligomeric Bcl-xL^{C110R1} was 36%, as calculated by comparing the second integral of the cw EPR spectra with a reference TEMPOL standard.
For Bax, the dialysate after the chitin column was loaded on an anion exchange column (HiTrap® Q High Performance) at 0.5 ml/min. The column was washed with Mono A buffer (8 mM Tris, pH 8.0) and the protein was eluted running a gradient with Mono B buffer (20 mM Tris, pH 8.0, 1 M NaCl) pooling the first peak.
To label wild type Bax (containing two natural cysteines C62 and C126), 10x excess MTSL per protein (protein concentration 10-20 µM) was added and incubated overnight at 4°C. The excess label was removed by washing 4-5x in centrifugal filters (Vivaspin® Turbo 4 Sartorius (cutoff 10 kDa)) with storage buffer. The spin labeling efficiency (spin per protein) of Bax^{R1} was 94% (spin per cysteine), as calculated by comparing the second integral of the cw EPR spectra with a reference TEMPOL standard (see SI).

For both, Bax and Bcl-xL, we found that using the Vivaspin® Turbo 4 Sartorius centrifugal filters caused less protein loss compared to other centrifugal filters. For Bcl-xL, removing excess label in spin desalting columns resulted in complete protein loss.
All proteins were tested in pore formation assays before further experimental use.

Mass photometry

Mass photometry was measured at different concentrations on a 2MP Mass Photometer from Refeyn in the Protein Production and Structure Core Facility at EPFL, Lausanne,

Switzerland.

LUVs Preparation

The lipid mixture mimicking the mitochondrial outer membrane was composed of 46% egg L-α-phosphatidyl choline (PC), 25% egg L-α phosphatidyl ethanolamine (PE), 11% bovine liver L-α-phosphatidyl inositol (PI), 10% 18:1 phosphatidyl serine (PS) and 8% cardiolipin (CL) (% w/w). The lipid mixture in chloroform was aliquoted, dried under vacuum, flushed with nitrogen and stored at -80°C for a maximum time of one year. To prepare large unilamellar vesicles the mix was solved in either storage buffer to give a stock solution of 20 mg/ml (for EPR experiments) or in calcein (80 mM, adjusted to pH 7.0 with NaOH, Sigma) (pore formation assays) using five freeze-and-thaw cycles and extruded 41x through a membrane with 400 nm pores. For the pore formation assays the LUVs were passed through a desalting column (Econo-Pac 10DG Desalting Columns , Biorad) equilibrated in outside buffer (20 mM HEPES, pH 7.0, 140 mM NaCl, 1 mM EDTA) to remove non-trapped calcein and diluted to a final maximum concentration of 1.25 mg/ml.

Pore-formation assays

Pore formation assays were performed at 37°C in outside buffer with maximum 0.02 mg/ml LUVs and protein concentrations of 25 nM. The fluorescence was monitored over time (excitation: 495 nm, emission: 520 nm), observing the fluorescence increase of the calcein trapped in LUVs due to the dequenching after being released in the surrounding buffer upon pore formation. To determine the maximum fluorescence (100% value), triton-X-100 (max. 0.05%) was added at the end of the fluorescence kinetic measurement. In all protein combinations, the inhibitor (Bcl-xL) was added first, then the pore former (Bax) and finally, the activator (cBid) in a 1:1:1 stoichiometric ratio.

Membrane sample preparation

All pellet/supernatant samples analyzed (SDS PAGE, CW EPR, DEER) have been prepared as described in fig. 3A. Proteins and LUVs were mixed with a final protein concentration of 10-20 μM and a final lipid concentration of 1-5 mg/ml. After one hour incubation at 37°C, the membrane and water sample were separated via centrifugation (120000xg). The pellet was resuspended and adjusted according to the methods requirements.

Continuous wave EPR

All continuous wave (cw) EPR experiments were performed on a Bruker E500 X-band equipped with a super high Q cavity ER 4122 SHQ with a power of 2 mW and a modulation amplitude of 0.1 or 0.15 mT.
For the time-resolved measurements, four spectra were averaged before moving to the next time point. The temperature was controlled at 37°C with a nitrogen flow cryostat and a temperature controller (Eurotherm). Samples were measured in a total volume of 20 µL in glass capillaries (Blaubrand). Proteins at 10-20 μM final concentrations were mixed on ice and introduced into the glass capillary. In a second step, a small volume of LUVs was added to the capillary. The first spectrum was detected after 2.5 min from the addition of LUVs to the protein mixture.

DEER measurements

The DEER experiments were performed on a Bruker Q-band Elexsys E580 spectrometer equipped with a 150 W TWT amplifier, a Bruker Spinjet-AWG, and a homemade probe head accommodating 3.0 mm o.d. tubes. Measurements were performed at 50 K. The sample temperature was controlled via a cryo-free system from Cryogenics.
We used the dead-time free 4-pulse DEER sequence with Gaussian pulses[23] (predefined pulse shape 1 in Bruker Xepr version 2.6b.170) and 16-step phase cycling. All pulses were adjusted to the same pulse length (32-34 ns corresponding to 16-20 ns FWHM) with the pump position at the maximum of the nitroxide spectrum and the observer at -90 MHz.
Table 1 summarizes the used parameters.

Table 1: Applied DEER parameters.

	NO-NO DEER
Shot repetition time [ms]	5
t_1 [ns]	400
t_2 [ns]	2000
Pump increasing step [ns]	8
8 t_1 averages in steps of [ns]	16

For DEER samples, the pellet (see membrane sample preparation) was resuspended in deuterated storage buffer and mixed with 10% d8-glycerol to the final sample volume of 40 µl. The samples were shock frozen in 3 mm o.d. quartz tubes (Aachener Quarzglas) and stored at -80°C. DEER data were analyzed with DeerAnalysis[24] 2021 using Tikhonov regularization and validation to obtain the uncertainties.

Negative stain electron microscopy and data analysis

3 μl of oligomeric Bcl-xL (0.05 mg/ml) were applied to a freshly glow discharged 400-mesh carbon-coated copper grid and incubated for 1 min before staining with 0.75% uranyl formate solution for 1 min. Grids were air dried for 5 min before they were imaged in a J1400 TEM (Jeol) equipped with a TVIPS 4k x 4k F416 detector.
36 micrographs recorded at 80,000x magnification (pixel size: 1.36 Å/px) were imported in CryoSPARC (version 4.7.0) and processed in negative stain mode with constant CTF. Particles were identified using the blob picker set to a diameter between 70 and 150 Å. 3,664 particles were extracted at a pixel size 2.72 Å/px and subjected to 2D classification using 36 classes to distinguish between intact oligomers and monomers.

Conflicts of interest

There are no conflicts to declare.

Data availability

All primary data are available upon request.

Acknowledgements

Technical support for protein purifications was provided by O. Vadas, R. Visentin, L. Falconet (Protein Platform, Faculty of Medicine, University of Geneva, Switzerland) and A. Cieren (Department of Physical Chemistry, Sciences II, University of Geneva, Switzerland). Technical support for mass photometry was provided by Y. Duhoo (Protein Production and Structure Core Facility, EPFL, Lausanne, Switzerland). Technical support during preliminary work was provided by J. Beermann and Dr. S. Bleicken (Ruhr University Bochum, Germany). EB and CE want to thank Prof. Dr. A. J. García-Sáez for providing the Bcl-2 plasmids. This work is supported by the SNSF Sinergia grant CRSII5_216587.

Bibliography

(1) Czabotar, P. E.; Lessene, G.; Strasser, A.; Adams, J. M. *Nature reviews. Molecular cell biology* **2014**, *15*, 49–63.

(2) Kale, J.; Osterlund, E. J.; Andrews, D. W. *Cell death and differentiation* **2018**, *25*, 65–80.

(3) Czabotar, P. E.; Garcia-Saez, A. J. *Nature Reviews Molecular Cell Biology* **2023**, DOI: `10.1038/s41580-023-00629-4`.

(4) Llambi, F.; Moldoveanu, T.; Tait, S. W. G.; Bouchier-Hayes, L.; Temirov, J.; McCormick, L. L.; Dillon, C. P.; Green, D. R. *Molecular cell* **2011**, *44*, 517–531.

(5) Kalkavan, H.; Green, D. R. *Cell Death & Differentiation* **2018**, *25*, 46–55.

(6) Billen, L. P.; Shamas-Din, A.; Andrews, D. W. *Oncogene* **2008**, *27 Suppl 1*, S93–104.

(7) Nguyen, D.; Osterlund, E.; Kale, J.; Andrews, D. W. *Biochemical Journal* **2024**, *481*, 903–922.

(8) Ding, J.; Mooers, B. H.; Zhang, Z.; Kale, J.; Falcone, D.; McNichol, J.; Huang, B.; Zhang, X. C.; Xing, C.; Andrews, D. W.; Lin, J. *Journal of Biological Chemistry* **2014**, *289*, 11873–11896.

(9) O'Neill, J. W.; Manion, M. K.; Maguire, B.; Hockenbery, D. M. *Journal of Molecular Biology* **2006**, *356*, 367–381.

(10) Czabotar, P. E.; Westphal, D.; Dewson, G.; Ma, S.; Hockings, C.; Fairlie, W. D.; Lee, E. F.; Yao, S.; Robin, A. Y.; Smith, B. J.; Huang, D. C. S.; Kluck, R. M.; Adams, J. M.; Colman, P. M. *Cell* **2013**, *152*, 519–531.

(11) Bogner, C.; Kale, J.; Pogmore, J.; Chi, X.; Shamas-Din, A.; Fradin, C.; Leber, B.; Andrews, D. W. *Molecular Cell* **2020**, *77*, 901–912.e9.

(12) Bleicken, S.; Wagner, C.; García-Sáez, A. J. *Biophysical journal* **2013**, *104*, 421–431.

(13) Ryzhov, P.; Tian, Y.; Yao, Y.; Bobkov, A. A.; Im, W.; Marassi, F. M. *Biophysical Journal* **2020**, *119*, 1324–1334.

(14) Bleicken, S.; Hantusch, A.; Das, K. K.; Frickey, T.; Garcia-Saez, A. J. *Nature communications* **2017**, *8*, 73.

(15) Rajan, S.; Choi, M.; Nguyen, Q. T.; Ye, H.; Liu, W.; Toh, H. T.; Kang, C.; Kamariah, N.; Li, C.; Huang, H.; White, C.; Baek, K.; Grüber, G.; Yoon, H. S. *Scientific Reports* **2015**, *5*, 10609.

(16) Denisov, A. Y.; Sprules, T.; Fraser, J.; Kozlov, G.; Gehring, K. *Biochemistry* **2007**, *46*, 734–740.

(17) Bleicken, S.; Classen, M.; Padmavathi, P. V. L.; Ishikawa, T.; Zeth, K.; Steinhoff, H.-J.; Bordignon, E. *The Journal of biological chemistry* **2010**, *285*, 6636–6647.

(18) Bleicken, S.; Assafa, T. E.; Stegmueller, C.; Wittig, A.; Garcia-Saez, A. J.; Bordignon, E. *Cell death and differentiation* **2018**, *25*, 1717–1731.

(19) Jeschke, G. *Protein science : a publication of the Protein Society* **2018**, *27*, 76–85.

(20) Schiemann, O. et al. *Journal of the American Chemical Society* **2021**, *143*, 17875–17890.

(21) Desagher, S.; Osen-Sand, A.; Nichols, A.; Eskes, R.; Montessuit, S.; Lauper, S.; Maundrell, K.; Antonsson, B.; Martinou, J.-C. *The Journal of Cell Biology* **1999**, *144*, 891–901.

(22) Suzuki, M.; Youle, R. J.; Tjandra, N. *Cell* **2000**, *103*, 645–654.

(23) Teucher, M.; Bordignon, E. *Journal of magnetic resonance (San Diego, Calif. : 1997)* **2018**, *296*, 103–111.

(24) Jeschke, G.; Chechik, V.; Ionita, P.; Godt, A.; Zimmermann, H.; Banham, J.; Timmel, C. R.; Hilger, D.; Jung, H. *Applied Magnetic Resonance* **2006**, *30*, 473–498.

(25) Teucher, M.; Zhang, H.; Bader, V.; Winklhofer, K. F.; García-Sáez, A. J.; Rajca, A.; Bleicken, S.; Bordignon, E. *Scientific Reports* **2019**, *9*, 3667.

Supplementary Information

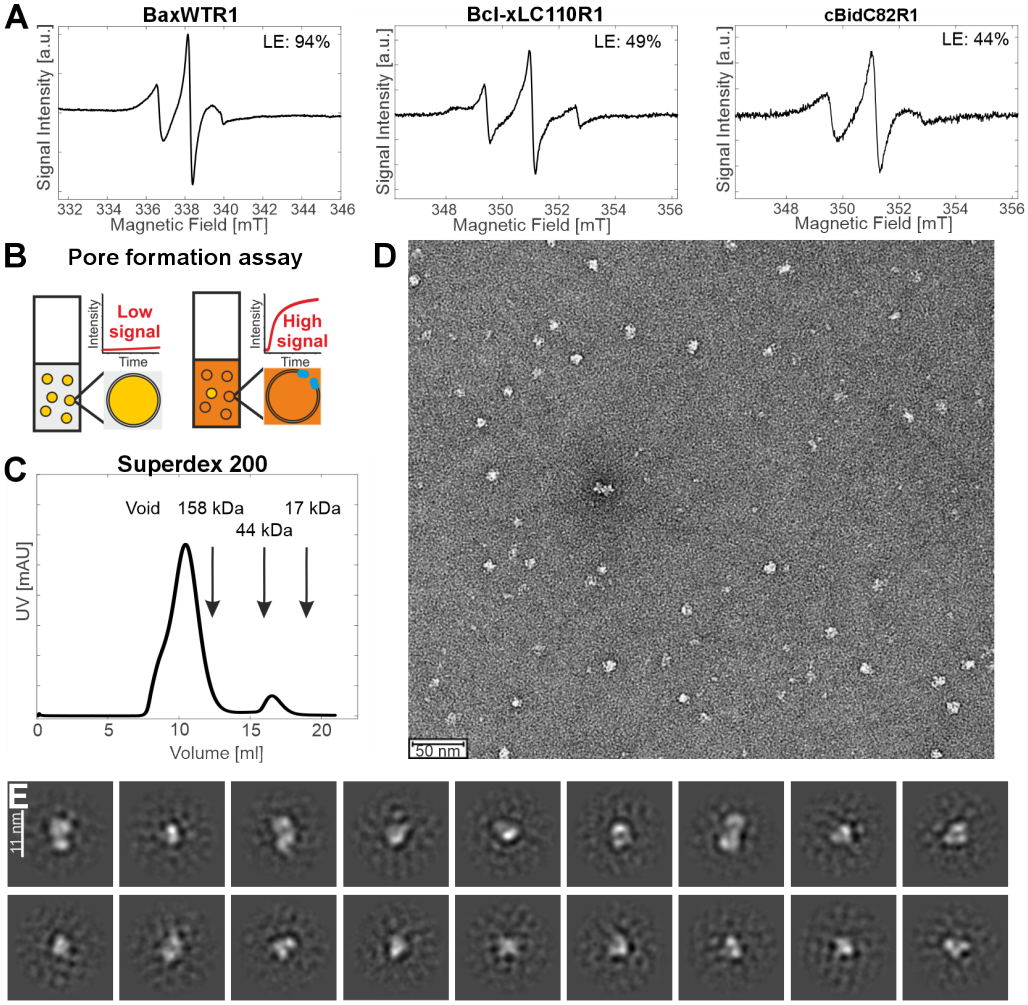

A: CW-EPR measurements and labeling efficiencies (spin per cysteine, LE) of all labeled proteins used. **B:** Graphic scheme of the fluorescence-based pore formation assays [25] (M. Teucher, H. Zhang, V. Bader, K. F. Winklhofer, A. J. García-Sáez, A. Rajca, S. Bleicken and E. Bordignon, Scientific Reports, 2019, 9, 3667.). When the calcein is trapped at high concentration (80 mM) in the LUVs, it self-quenches leading to a low fluorescence signal. Upon pore formation by Bax calcein is dilluted in the surrounding buffer, leading to an increase in fluorescence. **C:** SEC analysis of a Bcl-xL purification with a Superdex 200 10/300, with arrows highlighting masses of reference proteins. **D:** Representative EM figure of the negative staining. **E:** 2D class averages of 1380 particles of negative stain data representing smaller particles, likely monomers.